液体燃料—空气/氧气混合助燃超音速火焰喷涂枪的研制

贾 鹏, 王志平, 李 娜, 李亚娟
(中国民航大学 理学院, 天津 300300)

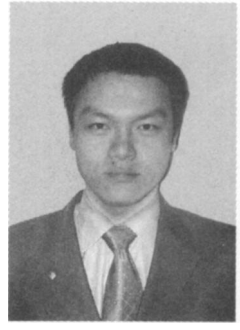

贾 鹏

摘 要: 采用枪内混气方式, 设计研制了一种采用炽热体作为稳焰器的液体燃料—空气/氧气混合助燃超音速火焰喷涂枪. 用 SprayWatch热喷涂监测系统测试喷涂枪焰流出口速度和温度, 并研究喷涂工艺对 WC-12Co涂层组织和性能的影响. 结果表明, 喷涂枪焰流出口速度超过 1 300 m/s, 焰流温度可在 2 302~3 410 K之间进行精确调节, 精度达到 ±50 K, 提高空气/氧气比, 涂层中 WC保留率明显提高, 使涂层硬度比氧气助燃时得到明显提高; 采用空气助燃进行喷涂, 可以得到厚度超过 5 mm的 WC-12Co涂层.

关键词: 超音速火焰喷涂枪; 稳焰器; 混合助燃; WC-12Co涂层
中图分类号: TG174.422 文献标识码: A 文章编号: 0253-360X(2010)06-0081-04

0 序 言

气体或液体燃料—氧气超音速火焰喷涂技术(high velocity oxygen fuel, HVOF)是继等离子喷涂之后又一次革命性进步, 其主要贡献在于大幅度提高涂层硬度和结合强度, 改善涂层中残余应力状态, 同时减少涂层中氧化物含量和孔隙率[1-3]; 但喷嘴的沉积堵塞、高额的涂层制作成本、喷涂材料易发生一定程度过热而氧化分解等诸多不利因素限制了 HVOF得到更为广泛的应用和发展[4,5]. 气体或液体燃料—空气超音速火焰喷涂技术(high velocity air fuel, HVAF)以压缩空气替代氧气进行助燃, 使燃烧室和喷涂焰流温度由 HVOF的 3 400 K降低到 2 400 K, 解决了 HVOF应用中很多难题, 但因喷涂焰流温度过低导致粉末沉积率下降, 并且受环境温度影响上下波动过大等不利因素导致 HVAF在工业生产中没有得到大规模应用.

为降低涂层制作成本, 解决枪嘴堵塞难题又不牺牲粉末沉积率最行之有效的办法是大范围精确调节和控制喷涂枪燃烧室和焰流温度, 使每种粉末都在最佳温度范围内进行喷涂. 作者的研究就是从这一需求出发, 研制出可调控液体燃料—空气/氧气混合助燃(以下简称 HVO/AF)的超音速火焰喷涂枪.

收稿日期: 2009-12-07
基金项目: 天津市科技发展计划科技攻关专项资助项目(043104011)

1 喷涂枪的研制

研制的 HVO/AF喷涂枪结构简图如图 1所示.

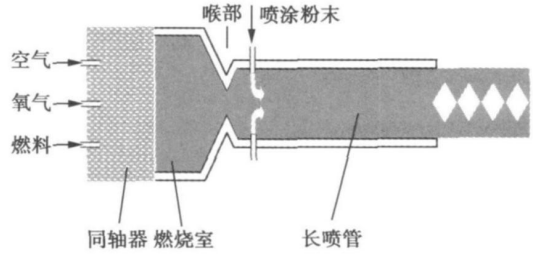

图 1 HVO/AF喷涂枪结构简图
Fig. 1 Schematic of HVO/AF gun

采用空气、氧气两种气体作为助燃剂, 关键在于两种助燃气体的混合和火焰的稳定性. 文中采用枪内混气方式解决两种助燃气体的混合问题, 该方式基本原理为采用独立控制系统分别控制空气和氧气的压力和流量, 将助燃气体通过单独气路导通到喷涂枪同轴稳定器, 并通过同轴稳定器上的气路使两种助燃气体进入燃烧室内部, 并与液体燃料充分混合, 燃烧形成稳定的高温高压气团, 得到超音速焰流, 完成喷涂.

为避免在低氧含量混合气体(特别是空气助燃时)燃烧时, 燃烧室由于水冷温度过低造成燃烧不连续不稳定, 文中采用炽热体作为稳焰器稳定燃烧

室的燃烧过程[6], 其原理为采用氧气助燃方式点燃燃烧室火焰后, 燃烧室高温烟气对稳焰器进行加热; 待稳焰器达到红热状态, 调节喷涂参数到设定值进行喷涂; 在喷涂过程中, 稳焰器从燃烧室高温烟气中吸收热量保持红热状态, 形成高温点火源, 稳定燃烧; 为避免稳焰器在高温烟气中熔化, 采用紫铜制作同轴稳定器将稳焰器的热量传递至冷却水, 并在稳焰器上开设空气气路. 液体燃料 -空气 /氧气枪助燃空气通道如图 2所示.

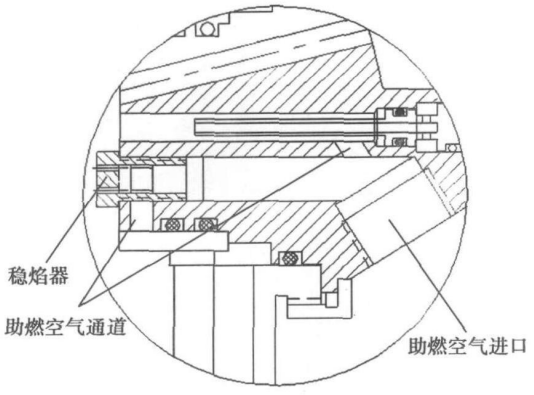

图 2 助燃空气通道及稳焰器示意图

Fig. 2 Schematic of air gallery and flameholder

2 试验方法

喷涂主机及送粉器采用自制的 JK3400型超音速火焰喷涂系统, 以航空煤油为燃料, 空气和氧气助燃. 喷涂粉末采用四川自贡硬质合金有限公司生产的 WC-12Co喷焊粉, 粉末粒度为 15~40 μm. 基体材料采用 45钢. 喷涂工艺参数见表 1.

表 1 HVO/AF喷涂工艺参数

Table 1 Parameters of HVO/AF

试样编号	氧气流量 q_o/(L·min^{-1})	空气流量 q_k/(L·min^{-1})	煤油流量 q_m/CCM	燃烧室压力 p/(MPa)
A	52 423	0	330	0.542(φ9燃烧室)
B	51 006	21 224	330	0.522(φ10燃烧室)
C	49 589	49 532	250	0.576(φ10燃烧室)
D	0	100 085	200	0.510(φ10燃烧室)

采用 SprayWatch热喷涂监测系统测试喷涂焰流出口速度和出口温度; 涂层的形貌特征分析采用 Quanta200型扫描电镜 (SEM); 涂层孔隙率采用 Axio imager A1m图像分析系统测定; 物相分析采用日本理学 Rigaku 2500/PC型 X射线衍射仪, 并用 XRD分析软件 (Jade5.0)计算 WC保留率; 涂层显微硬度测量采用 HVS-1000型显微硬度测量仪; 涂层结合强度测定采用 WE-10A万能材料试验机.

3 试验结果及分析

3.1 焰流出口速度、出口温度及沉积效率

喷涂焰流出口速度、出口温度及粉末沉积效率测定结果见表 2. 粉末沉积效率测定结果显示, HVO/AF喷涂枪沉积效率较常规 HVAF喷涂工艺沉积效率 (50%)高. 图 3给出了采用试样 A和试样 D喷涂工艺参数喷涂时所得到的喷涂焰流特征照片.

表 2 HVO/AF喷涂焰流出口速度、温度和沉积效率

Table 2 Velocity and temperature of jet and deposit efficiency of HVO/AF

试样编号	焰流出口速度 v/(m·s^{-1})	焰流出口温度 T/K	沉积效率 D(%)
A	1 688	3 410±18	69
B	1 307	3 320±27	67
C	1 433	2 934±34	63
D	1 305	2 302±47	58

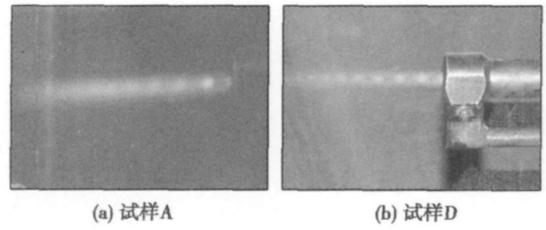

图 3 试样 A和 D喷涂工艺的喷涂焰流

Fig. 3 Photographs of jet for parameters of A and D

3.2 涂层的组织与性能分析

3.2.1 涂层形貌与孔隙率

HVO/AF喷涂的 WC-12Co涂层孔隙率测定结果如图 4所示, 涂层形貌如图 5所示. 由图 5可以看出, WC-12Co涂层非常致密, 在颗粒边缘未发现

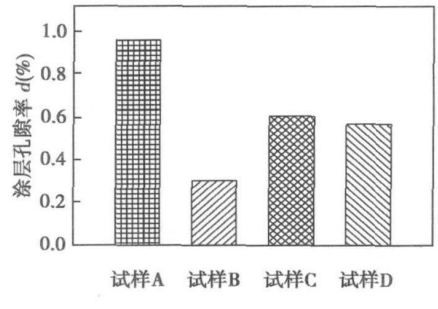

图 4 WC-12Co涂层孔隙率

Fig. 4 Porosity of WC-12Co coatings

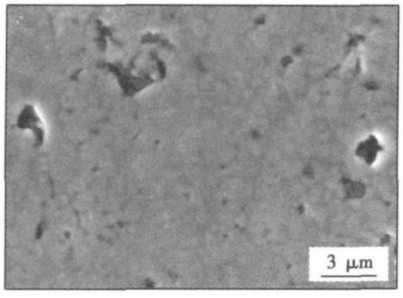

(a) 试样A涂层SEM形貌

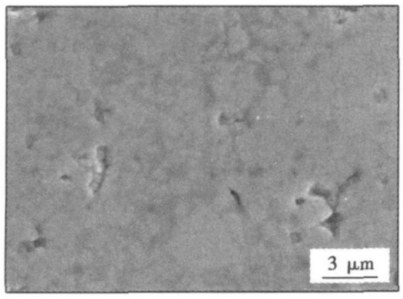

(b) 试样B涂层SEM形貌

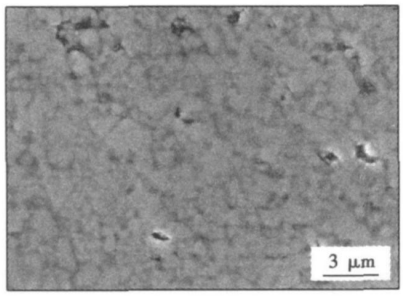

(c) 试样C涂层SEM形貌

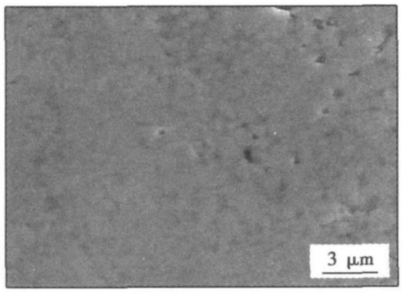

(d) 试样D涂层SEM形貌

图 5　WC-12Co涂层 SEM形貌

Fig. 5　SEM paragraphs of WC-12Co coatings

明显氧化物或显微裂纹,WC均匀地分布于涂层中.孔隙率测定结果显示试样 A涂层孔隙率最高,为 1.08%;试样 B涂层孔隙率最低,为 0.33%.

3.2.2　涂层硬度

超音速火焰喷涂 WC/Co涂层主要用于制备耐磨涂层,硬度是该涂层主要技术指标.同样是 WC-12Co涂层,由于喷涂工艺方法不同,其显微组织和相结构有很大差别,其硬度也有很大的差别.造成这种现象的主要原因是 WC颗粒在喷涂过程中很容易发生热分解、氧化和扩散.美国 Kemetico Inc公司公布的数据显示,该公司研制的 HVAF喷涂枪制备的 WC-12Co涂层硬度(维氏硬度)不超过 1 200 HV.WC-12Co涂层硬度试验结果(图 6)显示,研制的 HVO/AF喷涂枪制备的涂层硬度(维氏硬度)均达到或超过 1 500 HV.

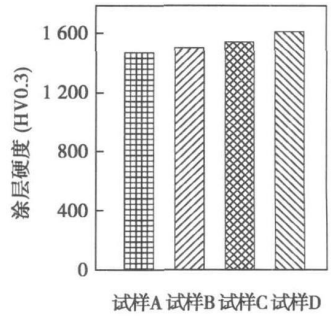

图 6　WC-12Co涂层显微硬度

Fig. 6　Microhardness of WC-12Co coatings

3.2.3　涂层 X射线衍射分析

X射线衍射分析结果(图 7,图 8)显示,WC-12Co粉末原始相为 WC,基本没有 W_2C和金属钨;采用纯氧气作为助燃剂制备的涂层相结构与粉末相近,但存在部分 W_2C金属钨,说明采用纯氧气作为助燃剂喷涂时,部分 WC颗粒发生分解和氧化;采用空气和氧气混合作为助燃剂制备的涂层也存在少量 W_2C,金属钨,但含量小于采用纯氧气作为助燃剂制备的涂层,而且空气含量越高,W_2C,金属钨含量越低,说明随着空气含量的增高,涂层中 WC分解率降低;采用空气作为助燃剂时,WC涂层相结构与粉末基本相同.这充分证实了助燃剂采用的空气量越大,火焰温度越低,喷涂粉末中 WC分解的可能性越低.图 9为 HVO/AF喷涂 WC-12Co涂层 WC保留率.

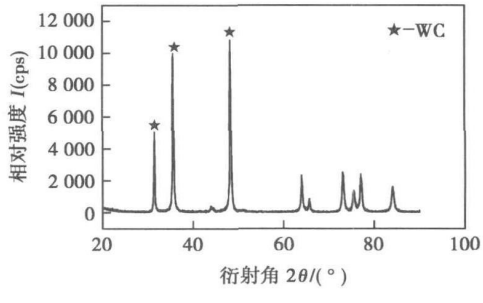

图 7　WC-12Co粉末 XRD衍射谱线

Fig. 7　XRD pattern of WC-12Co powder

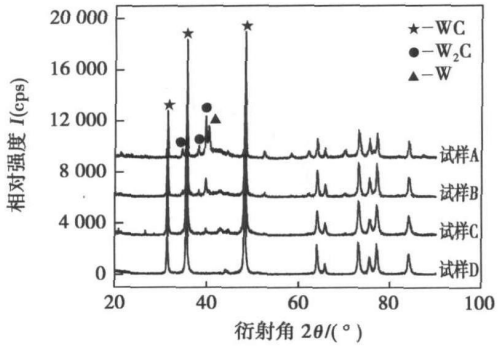

图 8 WC-12Co 涂层 XRD 衍射谱线

Fig. 8 XRD patterns of WC-12Co coatings

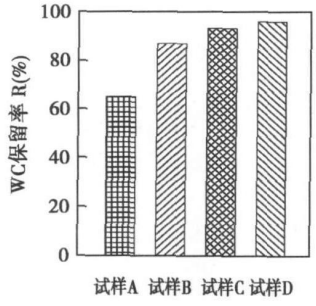

图 9 WC-12Co 涂层 WC 保留率

Fig. 9 WC retention rate of WC-12Co coatings

3.2.4 涂层大厚度试验

美国 Kemetico Inc公司研制的 HVAF喷涂枪制备的 WC-12Co最大厚度为 2 mm. 作为对比, 试验采用试样 D喷涂参数喷涂涂层大厚度试样 (图 10). 当涂层厚度达到 5.11 mm时, 涂层未出现剥落现象, 说明采用该工艺参数的喷涂颗粒具有很高的飞行速度, 涂层残余应力状态为压应力[7], 涂层中颗粒之间连接紧密, 具有很高的结合强度, 优于 Kemetico Inc公司研制的 HVAF喷涂枪, 极大扩展了热喷涂涂层的应用范围.

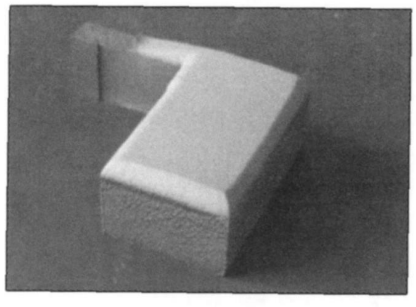

图 10 大厚度涂层试样

Fig. 10 Photograph of heavy gauge coating

4 结 论

(1) 采用炽热体作为火焰稳定器得到稳定燃烧的液体燃料—空气/氧气混合助燃超音速火焰, 首次实现了空气/氧气混合助燃、枪内混气方式进行超音速火焰喷涂.

(2) 该枪采用调节空气/氧气比例实现在 3 400 K至 2 400 K之间进行大范围高精度调节喷涂焰流温度, 精度达到 ±50 K, 喷涂焰流速度超过 1 300 m/s.

(3) 提高空气/氧气比例, 可以明显提高 WC-12Co涂层中 WC的保留率, 使涂层硬度比氧气助燃时得到明显提高.

(4) 采用空气助燃进行超音速喷涂, 可以得到厚度超过 5 mm的 WC-12Co涂层, 极大扩展了热喷涂涂层的应用范围.

参考文献:

[1] Moskowitz L N. Application of HVOF thermal spraying to solve corrosion problems in the petroleum-An industry note[J]. Journal of Thermal Spraying Technology, 1993(1): 21—29.

[2] 王志平, 霍树斌, 刘 瑾. 超音速火焰喷涂 (HVOF)技术的发展与工艺特点[J]. 焊接, 2000(6): 6—10.
Wang Zhiping, Huo Shubin, Liu Jin. Development and characteristics of high velocity oxygen-fuel (HVOF) spray[J]. Welding & Joining, 2000(6): 6—10.

[3] Voorwald H J C, Souza R C. Evaluation of WC-17Co and WC-10Co-4Cr thermal spray coatings by HVOF on the fatigue and corrosion strength of AISI4340 steel[J]. Surface and Coatings Technology, 2005(190): 155—164.

[4] Zimmermann S, Keller H, Schwier G. New Carbide based materials for spraying[C] // Thermal Spray 2003: Advancing the Science & Applying the Technology. Ohio, USA: AMS International Materials Park, 2003: 227—233.

[5] Qiao Y F, Fischer T E, Dent A. The effects of fuel chemistry and feedstock powder structure on the mechanical and tribological properties of HVOF thermal sprayed WC-Co coatings with very fine structures[J]. Surface and Coatings Technology, 2003, 172: 24—41.

[6] 钱申贤. 燃气燃烧原理[M]. 北京: 中国建筑工业出版社, 1989.

[7] Verstak A, Baranovski V. Deposition of carbides by activated combustion HVAF spraying[C] // Proceedings of the International Thermal Spray Conference. Osaka, Japan, 2004: 551—555.

作者简介: 贾 鹏, 男, 1980年出生, 硕士, 实验师. 主要从事材料学方面的科研和教学工作. 发表论文 16篇.

Email: pjia@cauc.edu.cn

structure; low temperature impact resistance

Property analysis and brazing preparation of NiTi/NiTiNb composite sheet ZHAO Xingke, TANG Jiawei, HUANG Jihua, ZHANG Hua (School of Materials Science and Engineering, Beijing Science and Technology University, Beijing 100083, China). p. 73—76, 80

Abstract: The microstructure of interface and bending deformation behavior of composite sheet which was brazed by AgCu eutectic brazing alloy were investigated. The results reveal that the brazing joint has good mechanical properties, and the bending angle of the brazed plates reaches 120° at room temperature or 0 ℃ without fracture. The composite sheet shows good shape memory effect, and the shape recovery temperature has a larger range between the shape recovery temperatures of these two alloys, which is resulted by the deformation compatibility of the two alloys. The stress-strain curves of the composite sheet show obvious hysteretic loop and indicate good damping characteristic at room temperature or 0 ℃.

Key words: brazing; shape memory alloy composite sheet; stress-strain

Microstructure and solderability of Sn-9Zn-xCe lead-free solder HU Yuhua, XUE Songbai, CHEN Wenxue, WANG Hui (College of Materials Science and Technology, Nanjing University of Aeronautics and Astronautics, Nanjing 210016, China). p. 77—80

Abstract: Effects of rare earth element Ce added in Sn-9Zn solder on the microstructure and spreading property as well as mechanical properties were investigated. Results indicate that with the increase of the Ce from 0 to 0.08%, the microstructure is refined obviously and Zn-rich Phrase is decreased. While the content of Ce exceeds 0.08%, small block Sn-Ce intermetallic compounds will appear. Results also show that with the increase of the Ce, the spreading property is improved, the spreading area reaches maximum when the content of Ce is up to 0.08%, and the best mechanical properties of the soldered joints are achieved while the content of Ce is about 0.08%.

Key words: rare earth element Ce; lead-free solder Sn-Zn; spread ability; mechanical properties; microstruture

Design of supersonic flame spraying gun with combustion-supporting of air-oxygen and liquid fuel JIA Peng, WANG Zhiping, LIN Na, LI Yajuan (College of Science, Civil Aviation University of China, Tianjin 300300, China). p. 81—84

Abstract: A supersonic flame spraying gun in which liquid fuel and air-oxygen are mixed in chamber to improve combustion stability by flameholder was obtained. The speed and temperature of jet from the gun was measured by the Spraywatch monitor system. The microstructure and properties of the WC-12Co coatings produced by the gun were investigated. The results indicate that the jet speed exceeds 1 300 m/s and the adjustable range of temperature is 2 302 K to 3 410 K, which an accuracy of adjustment reaches ±50 K. The WC retention rate in the coating increases with the increasing of air and oxygen mixing ratio and so the hardness of coatings increases. The thickness of the coating obtained by spraying with air-supporting combustion is over 5 mm.

Key words: supersonic flame spraying gun; flameholder; air-oxygen combustion-supporting; WC-12Co coating

Effects of aging on shearing strength and fracture surface characteristics of SnCuSb/Cu soldering joint MENG Gongge, LI Dan, LI Zhengping, WANG Yanpeng, CHEN Leida (1. School of Material Science & Engineering, Harbin University of Science and Technology, Harbin 150040, China; 2. School of Material Science & Engineering, Dalian University of Technology, Dalian 116024, Liaoning, China). p. 85—88

Abstract: The effects of 150 ℃ aging on the shearing strength and fracture surface characteristics of Sn-0.7Cu-xSb/Cu (x=0, 0.25, 0.5, 0.75, 1.0) soldering joints were studied by scanning electron microscopy and energy dispersive X-ray spectrometry. The results indicate that the shearing strength of the joint increases with the increasing of Sb in solder and reduces remarkably with the increasing of aging time. The location of fracture is at the solder and appears at interface between the solder and the intermetallic compound of Cu_6Sn_5. Fracture for post soldering specimen with a lot of dimples on its surfaces occurs mainly at the solder and the fracture type is ductile. With the increasing of aging time, the fracture location trends to half solder and half interfacial intermetallic compound. In 500 h aging, Cu_3Sn can be seen at fracture surface which transfers to brittleness from ductileness.

Key words: soldering joints; shearing strength; aging; fracture surface; SnCuSb

Microstructure and corrosion resistance of butt joint of 1Cr18Ni9Ti+Q235 composite plate WANG Wenxian, WANG Yifeng, LIU Mancai, CHENG Fuchang, WU Wei (1. College of Materials Science and Engineering, Taiyuan University of Technology, Taiyuan 030024, China; 2. Taiyuan Yangguanyuan Stainless Steel Co., Ltd., Taiyuan 030008, China). p. 89—92

Abstract: Four different automatic welding techniques were applied for butt welding of the composite pipe that has a clad layer of 1Cr18Ni9Ti with a thickness of 3 mm and a substrate layer of Q235 with a thickness of 10 mm. The properties of the joint including microstructure, tensile strength, bend strength, impact toughness, electrochemical and intergranular corrosion resistance were evaluated. The results indicate that the phase of the clad layer welded by tungsten inert gas welding (TIG) is austenite with a little ferrite. The electrochemical corrosion resistance of the joint is similar to that of the base metal in hydrochloric acid of 1 mol/L and no intergranular corrosion is observed. The phase of the TIG welded joint of the substrate layer is martensite laths that have high strength and excellent toughness. But both the joints of the substrate layer and the clad layer welded by submerged arc welding have poorer mechanical properties and corrosion resistance, respectively.

Key words: stainless steel composite plate; welding technique; mechanical properties; corrosion resistance

Analysis of dynamic and residual stresses in overlaying process of large frame construction ZHONG Zhiyong, FU Wei, GU Yirong, BI Gang (Baosteel Equipment Maintenance Co., Ltd., Baosteel Machinery Factory, Shanghai 201900, Chi-